BJP British Journal of Pharmacology

DOI:10.1111/bph.12840
www.brjpharmacol.org

RESEARCH PAPER

TRPC6 regulates cell cycle progression by modulating membrane potential in bone marrow stromal cells

Jun Ichikawa and Ryuji Inoue

Department of Physiology, School of Medicine, Fukuoka University, Fukuoka, Japan

Correspondence
Jun Ichikawa, Department of Physiology, School of Medicine, Fukuoka University, 7-45-1 Nanakuma, Jonan-ku, Fukuoka 814-0180, Japan. E-mail: ichikawaj@fukuoka-u.ac.jp

Received
15 December 2013
Revised
26 June 2014
Accepted
1 July 2014

BACKGROUND AND PURPOSE

Ca^{2+} influx is important for cell cycle progression, but the mechanisms involved seem to vary. We investigated the potential roles of transient receptor potential (TRP) channels and store-operated Ca^{2+} entry (SOCE)-related molecules STIM (stromal interaction molecule)/Orai in the cell cycle progression of rat bone marrow stromal cells (BMSCs), a reliable therapeutic resource for regenerative medicine.

EXPERIMENTAL APPROACH

PCR and immunoblot analyses were used to examine mRNA and protein levels, fluorescence imaging and patch clamping for Ca^{2+} influx and membrane potential measurements, and flow cytometry for cell cycle analysis.

KEY RESULTS

Cell cycle synchronization of BMSCs revealed S phase-specific enhancement of TRPC1, STIM and Orai mRNA and protein expression. In contrast, TRPC6 expression decreased in the S phase and increased in the G_1 phase. Resting membrane potential (RMP) of BMSCs was most negative and positive in the S and G_1 phases, respectively, and was accompanied by an enhancement and attenuation of SOCE respectively. Chemically depolarizing/hyperpolarizing the membrane erased these differences in SOCE magnitude during the cell cycle. siRNA knockdown of TRPC6 produced a negative shift in RMP, increased SOCE and caused redistribution of BMSCs with increased populations in the S and G_2/M phases and accumulation of cyclins A2 and B1. A low concentration of Gd^{3+} (1 μM) suppressed BMSC proliferation at its concentration to inhibit SOC channels relatively specifically.

CONCLUSIONS AND IMPLICATIONS

TRPC6, by changing the membrane potential, plays a pivotal role in controlling the SOCE magnitude, which is critical for cell cycle progression of BMSCs. This finding provides a new therapeutic strategy for regulating BMSC proliferation.

Abbreviations

CPA, cyclopiazonic acid; FUCCI, fluorescent ubiquitination-based cell cycle indicator; NMDG, *N*-methyl-D-glucamine; OAG, 1-oleoyl-2-acetyl-*sn*-glycerol; Pyr2, pyrazole compound-2; RMP, resting membrane potential; SOC, store-operated channel; SOCE, store-operated Ca^{2+} entry; STIM, stromal interaction molecule; TRP, transient receptor potential; TRPC, canonical TRP

Table of Links

TARGETS	LIGANDS
Akt (PKB)	Cyclopiazonic acid
CDK	5-fluorouracil
M_2 receptor	Gd^{3+}
TRPC1	OAG
TRPC6	Thymidine
TRPM5	

This Table lists key protein targets and ligands in this document, which are hyperlinked to corresponding entries in http://www.guidetopharmacology.org, the common portal for data from the IUPHAR/BPS Guide to PHARMACOLOGY (Pawson *et al.*, 2014) and are permanently archived in the Concise Guide to PHARMACOLOGY 2013/14 (Alexander *et al.*, 2013a,b,c).

Introduction

Bone marrow stromal cells (BMSCs) are non-haematopoietic cells residing in the bone marrow cavity (Krebsbach *et al.*, 1999). BMSCs include mesenchymal stem cells (MSCs), which differentiate into osteoblasts, adipocytes and chondrocytes *in vitro*, and thus can be used as a reliable therapeutic resource for regenerative medicine and bioengineering (Prockop, 1997; Pittenger *et al.*, 1999; Uccelli *et al.*, 2008). Controlling the proliferative potential and cell cycle progression of MSCs is an attractive approach to maximizing the yield of MSCs during expansion *in vitro*. In addition, identifying the cell cycle-driving machinery or mechanism of MSCs will increase our understanding of stem cell-specific properties such as self-renewal and multilineage differentiation potential (Caplan, 2007). It is known that intracellular signalling activated by growth factors/hormones and cytokines is crucial for the growth and differentiation of MSCs (Pricola *et al.*, 2009), but the mechanisms underlying these processes remain poorly understood.

Intracellular Ca^{2+} regulates a multitude of cellular events including fertilization, contraction, cell growth and differentiation (Berridge *et al.*, 2003). Ca^{2+} influx via both voltage-gated and non-voltage-gated Ca^{2+} entry channels plays important roles in cell cycle progression in many types of cells (Beech, 2007; Oguri *et al.*, 2010). Transient receptor potential (TRP) and store-operated (SOC) channels are recognized as the main families of non-voltage-gated Ca^{2+} channels (Elliott, 2001). Mammalian TRP channels are classified into six subfamilies (TRPC, TRPM, TRPV, TRPP, TRPA and TRPML) and are activated by various physicochemical stimuli (Nilius *et al.*, 2007). TRPC channels are activated by stimulation of PLC-coupled receptors via generation of DAG or depletion of intracellular Ca^{2+} stores (Nilius *et al.*, 2007) and permeate both Na^+ and Ca^{2+}. SOC channels can be activated by store depletion *per se* irrespective of receptor stimulation and show a high selectivity for Ca^{2+} (Parekh, 2007). Many recent studies have proposed that STIM (stromal interaction molecule)/Orai families are the main pore-forming/regulatory molecules responsible for SOC channels (Cahalan, 2009). Several reports have demonstrated that TRP/SOC channels contribute to cell growth regulation (Abdullaev *et al.*, 2008; Cheng *et al.*, 2010; El Boustany *et al.*, 2010; Armisén *et al.*, 2011; Becchetti, 2011; Dhennin-Duthille *et al.*, 2011), but the mechanism(s) involved therein seems variable depending on the cell type.

In this study, we explored the roles of TRP channels and store-operated Ca^{2+} entry (SOCE)-related molecules, STIM and Orai, in the Ca^{2+}-dependent regulation of cell cycle progression of BMSCs. We found that, in the S phase, the expression levels of TRPC1, STIM and Orai were significantly increased together with the increased magnitude of SOCE, whereas that of TRPC6 was markedly reduced. Furthermore, membrane potential measurement and flow cytometric cell cycle analysis combined with siRNA knockdown techniques suggested that the transmembrane gradient for Ca^{2+} influx, which is effectively regulated by the depolarizing activity of TRPC6, is critical for BMSC proliferation.

Methods

Cell culture

All animals were handled in accordance with the 'Rules of Animal Experimentation Committee, Fukuoka University School of Medicine'. Standard culture medium was Eagle's minimum essential medium with Eagle's salts (E-MEM; Wako, Tokyo, Japan) supplemented with 10% heat-inactivated FBS (Nichirei Biosciences Inc., Tokyo, Japan) and antibiotics (100 $U \cdot mL^{-1}$ penicillin, 100 $\mu g \cdot mL^{-1}$ streptomycin and 0.25 $\mu g \cdot mL^{-1}$ amphotericin B; Sigma-Aldrich, St. Louis, MO, USA).

The isolation and culture of BMSCs were performed as described previously (Ichikawa and Gemba, 2009). Briefly, BMSCs were isolated from the femoral shaft of male Fischer 344 rats (6 or 7 weeks old; CLEA Japan, Inc., Tokyo, Japan). Both ends of the femurs were cut at the epiphyses and the marrow was flushed out using 10 mL of culture medium expelled from a syringe through a 21 gauge needle. The bone marrow suspensions were cultured in 75 cm^2 culture flasks. Culture medium was changed 24 h later to remove non-adherent cells and subsequently renewed every 2–3 days. Adherent cells were allowed to grow as a monolayer in a humidified atmosphere at 5% CO_2 and 37°C for 1–2 weeks until reaching confluency. Cells were then dissociated using trypsin and replated on coverslips (0.12–0.17 mm thickness and 4 × 6 mm in size; Matsunami, Osaka, Japan) for fluorescence digital imaging and patch-clamping experiments, or maintained in culture dishes for other assays.

Cell cycle synchronization

After serum deprivation for 24–48 h in 0.1% FBS-containing MEM, cells were stimulated for 4 days using the following cell cycle-arresting drugs dissolved in 10% FBS-containing medium; mimosine (0.4 mM), thymidine (10 mM), 5-fluorouracil (400 μM) and demecolcine (60 ng·mL^{-1}) for the G_1, S, G_2 and M phases respectively.

Expression of FUCCI (fluorescent ubiquitination-based cell cycle indicator)

To visualize cell cycle stages of each cell tested, the Premo™ FUCCI Cell Cycle Sensor (Invitrogen, Carlsbad, CA, USA) was used according to the manufacturer's instructions. To detect geminin-GFP (S, G_2 and M phases) and Cdt1-RFP (G_1 phase) fluorescence, a set of multiband filters (DAPI/FITC/TRITC, Semrock, Lake Forest, IL, USA) were equipped on a fluorescence microscope.

siRNA procedure

Stealth™ siRNA duplexes specific for targeted proteins (Invitrogen) were transfected to BMSCs using Lipofectamine 2000 (Invitrogen), according to the manufacturer's instructions. For a negative control, we used Stealth RNAi duplexes (Invitrogen) with minimal sequence homology to any vertebrate transcripts and medium GC content.

Quantitative real-time PCR

Total RNA was isolated using the 'RNAeasy' mini kit (Qiagen, Venlo, the Netherlands) and cDNA was synthesized from total RNA using the 'high capacity cDNA reverse transcription kit' (Applied Biosystems, Foster City, CA, USA) according to the manufacturer's instructions. Quantitative real-time PCR was performed using the 7500Fast real-time PCR system (Applied Biosystems) according to the manufacturer's instructions. The sequences of oligonucleotide primers used for the amplification reaction are described in Supporting Information Table S1. Rat 18SrRNA, an endogenous housekeeping gene, was used as an internal control to assess the overall cDNA content. Amplification was performed in a final volume of 20 μL, which contained templates, primers and the Power SYBR® Green PCR Master Mix (Applied Biosystems). The amplification programme was as follows: 95°C for 10 min followed by 40 cycles of 95°C for 15 s and 60°C for 1 min. The operating software of the 7500Fast real-time PCR system was used for automated data collection and data analysis. The analysed data are presented as ratios compared with the controls. At least five independent experiments in four rats were performed.

Immunoblotting

Total cell lysates from BMSCs were prepared in sample buffer. The total protein concentration of the sample was determined using the bicinchoninic acid protein assay kit (Pierce, Rockford, IL, USA). Before electrophoresis, 5% (v/v) 2-mercaptoethanol and 1% (w/v) bromophenol blue were added to the sample, and proteins were separated by 10% (w/v) SDS-PAGE and electrophoretically transferred to a PVDF membrane. The membrane was blocked with 5% (w/v) skimmed milk dissolved in Tween-PBS and then incubated with appropriate primary antibodies diluted as recommended by the manufacturers. Protein expression was visualized by incubating the membrane with a secondary antibody conjugated with HRP.

Proliferation assay

To assay cell numbers, WST-8 [2-(2-methoxy-4-nitrophenyl)-3-(4-nitrophenyl)-5-(2,4-disulfophenyl)-2H-tetrazolium, monosodium salt], known commercially as the 'Cell Counting Kit-8' (Dojindo, Kumamoto, Japan), was used according to the manufacturer's instructions. The colourless substrate WST-8 was reduced by intracellular dehydrogenase to water-soluble, orange-coloured formazan. The amount of formazan could be directly measured spectrophotometrically at 450 nm. Cells cultured in 96-well plates were incubated with the Cell Counting Kit-8 for 90 min at 37°C and then the absorbance at 450 nm was measured in triplicate wells using a microplate reader (TriStar LB941, Berthold Technologies, Bad Wildbad, Germany).

Flow cytometry

Cells were harvested by trypsinization, washed with PBS and then incubated in propidium iodide/Triton X-100 staining solution with RNase A for 10 min at room temperature. The DNA content of stained cells was measured using a flow cytometer (FACSCanto II, BD Biosciences, San Jose, CA, USA) and its cell cycle-dependent distribution was analysed using the ModFit LT 3.0 software.

Measurement of $[Ca^{2+}]_i$ and membrane potential

The intracellular Ca^{2+} concentration ($[Ca^{2+}]_i$) was monitored by use of a digital fluorescence imaging technique. Briefly, cells plated on a glass coverslip were loaded with fura 2-acetoxymethyl ester (2 μM) at 37°C for 30 min. With alternating excitations at 340 and 380 nm, the intensity of fura 2 fluorescence emitted at 510 nm (±10 nm) was measured using a digital fluorescence image analysis system consisting of an inverted fluorescence microscope (DMI600B; Leica Microsystems GmbH, Wetzlar, Germany) and a low-noise, high-intensifying EMCCD camera (QuantEM 512SC, Photometrics, Tucson, AZ, USA). Data acquisition and analysis were performed using the software SlideBook 4.2 (Intelligent Imaging Innovation, Inc., Denver, CO, USA). The fluorescence values obtained were corrected for background fluorescence and autofluorescence, and changes in $[Ca^{2+}]_i$ were defined as the ratio of corrected fluorescence intensities at 340 and 380 nm (F_{340}/F_{380}).

For the measurement of membrane potential, cells were loaded with $DiBAC_4(3)$ (2 μM) at 37°C for 30 min. The intensity of $DiBAC_4(3)$ fluorescence emitted at 510 nm with 488 nm excitation was measured using the same system as described for $[Ca^{2+}]_i$ measurement.

Electrophysiology

Membrane currents were recorded using the tight-seal, whole-cell patch-clamp technique. Patch electrodes with a resistance of 4–6 MΩ (when filled with internal solution) were made from 1.5 mm borosilicate glass capillaries using an automated electrode puller (Sutter Instrument, Novato, CA, USA) and heat-polished. Voltage generation and current signal acquisition were performed using a patch-clamp amplifier (EPC-10,

HEKA Electronics, Lambrecht/Pfalz, Germany) controlled by the PatchMaster v. 2 × 53 software (HEKA Electronics). Current clamp recordings were performed with an A/D-, D/A-converter MacLab/4e (ADInstruments, Dunedin, New Zealand) and data evaluation was made by the Chart v. 4.2 software (ADInstruments). Cells showing a leak more negative than –5 pA at –60 mV after the establishment of whole-cell conditions were not included in the evaluation because the artificial leak seriously affected the value of the resting membrane potential (RMP). The pipette solution consisted of (mM): 140 KCl, 2 $MgCl_2$, 1 EGTA, 10 HEPES, 2 ATP, 0.1 GTP, 10 glucose (adjusted to pH 7.2 with Tris base). Bath solution consisted of (mM): 140 NaCl, 5 KCl, 1.2 $MgCl_2$, 1.8 $CaCl_2$, 10 HEPES, 10 glucose (adjusted to pH 7.4 with Tris base). Test solutions were rapidly applied using a handmade solenoid-driven fast solution change device 'Y-tube'. For perforated patch-clamp recording, an aliquot of the stock solution of nystatin (Calbiochem, Darmstadt, Germany) dissolved in methanol (5 mg·mL^{-1}) was diluted 25 times in pipette solution and ultrasonicated immediately before use. Nystatin-suspending pipette solution was filtered to remove undissolved nystatin aggregates. Approximately 1–2 min after 'giga' seal formation, a sufficiently low access resistance (typically < 20 MΩ) was attained using nystatin-mediated membrane perforation.

Solutions

Standard bath solution used for fluorescence imaging consisted of (mM): 140 NaCl, 5 KCl, 1.2 $MgCl_2$, 1.8 $CaCl_2$, 10 HEPES, 10 glucose (adjusted to pH 7.4 with Tris base). Ca^{2+}-free solution consisted of (mM): 140 NaCl, 5 KCl, 1.2 $MgCl_2$, 1 EGTA, 10 HEPES, 10 glucose (adjusted to pH 7.4 with Tris base). High-K^+ solution consisted of (mM): 45 NaCl, 100 KCl, 1.2 $MgCl_2$, 1.8 $CaCl_2$, 10 HEPES, 10 glucose (adjusted to pH 7.4 with Tris base). Na^+-free-external solution [*N*-methyl-D-glucamine (NMDG) solution] was made by equimolar substitution of Na^+ with NMDG.

Drugs and antibodies

Drugs for cell cycle synchronization (mimosine, thymidine, 5-fluorouracil and demecolcine) were purchased from Sigma-Aldrich. Gadolinium chloride was purchased from Sigma-Aldrich and cyclopiazonic acid (CPA) from Calbiochem. 1-Oleoyl-2-acetyl-*sn*-glycerol (OAG) was purchased from Cayman Chemical (Ann Arbor, MI, USA). Pyrazole compound-2 (Pyr2) was kindly supplied by Professor Yasuo Mori of Kyoto University.

Antibodies against TRPC1 and TRPC6 were purchased from Alomone labs (Jerusalem, Israel). Other antibodies were as follows: anti-STIM1 (Sigma-Aldrich), anti-STIM2 and anti-Orai3 (AnaSpec, Fremont, CA, USA), anti-Orai1 and anti-Orai2 (Osenses, Keswick, Australia), anti-phospho-Akt, anti-Akt and anti-cyclin D1 (Cell Signaling Technology, Danvers, MA, USA) and anti-β-actin (Abcam, Cambridge, UK).

Statistical analysis

All data are expressed as means ± SEM. For a single comparison, Student's unpaired *t*-test was used to evaluate statistical significance. For multiple comparisons, statistical significance was evaluated by one-way ANOVA followed by Tukey–Kramer or Steel–Dwass multiple comparison *post hoc* tests.

Results

Cell cycle-dependent expression of TRPC and STIM/Orai

We first analysed the expression of TRPC, STIM and Orai subtypes in rat BMSCs using conventional reverse transcription-PCR with subtype-specific primers (Supporting Information Table S1). As shown in Figure 1A, BMSCs express TRPC1, TRPC6 and all subtypes of STIM (STIM1, STIM2) and Orai (Orai1, Orai2, Orai3). To compare their mRNA levels at different cell cycle stages, we next carried out quantitative real-time PCR analyses in cell cycle-synchronized cultures. The total number of phase-arrested cells was significantly smaller than that of the control, but there was little noticeable increase in the number of dead cells (Figure 1B). Synchronization procedures (see the Methods section) significantly increased the fraction of cells arrested in each cell cycle phase (Figure 1C,D). The mRNA levels of TRPC1, STIM and Orai increased several fold in the S phase, but tended to decrease during the G_1 phase (Figure 1E). Quite oppositely, however, the TRPC6 mRNA level was significantly decreased in the S phase ($P < 0.01$, Figure 1E), but increased in the G_1 phase ($P < 0.001$, Figure 1E). This expression pattern was also confirmed at the protein level by immunoblotting (Figure 1F). These results imply that, compared with the other molecules related to Ca^{2+} mobilization (i.e. TRPC1 and STIM/Orai), TRPC6 may play a unique role in BMSC cell cycle progression.

Cell cycle-dependent Ca^{2+} channel activities

To elucidate the functional significance of differences observed upon cell cycle synchronization, we performed Ca^{2+}-imaging experiments. The magnitude of Ca^{2+} influx induced by reintroduction of Ca^{2+} following store depletion (SOCE) was largest in the S phase, whereas smallest in the G_1 phase (Figure 2A,B). The opposite pattern was observed for Ca^{2+} influx induced by the application of a membrane-permeable DAG analogue OAG (Figure 2C,D). These results clearly indicate the cell cycle dependence of store depletion- and DAG-activated Ca^{2+}-transporting activities, which paralleled the expression levels of their molecular correlates (see the former section Cell cycle-dependent expression of TRPC and STIM/Orai), that is TRPC1 or STIM/Orai and TRPC6 respectively (Hofmann *et al.*, 1999; Potier and Trebak, 2008; Vaca, 2010).

We also compared the effects of cell cycle synchronization on the basal $[Ca^{2+}]_i$ level, in the presence and absence of external Ca^{2+} without CPA treatment. In the presence of external Ca^{2+}, basal $[Ca^{2+}]_i$ was not significantly different among different cell cycle stages [F_{340}/F_{380} = 0.89 ± 0.050, 0.92 ± 0.075, 0.90 ± 0.080 and 0.88 ± 0.060 in the G_1, S, G_2 and M phases, respectively; each value represents the average of the means (from 50 to 60 cells) of four independent experiments]. However, when external Ca^{2+} was removed, basal $[Ca^{2+}]_i$ decreased significantly less in the G_1 phase compared with other phases [$P < 0.05$ by ANOVA with Tukey–Kramer test; $\Delta F_{340}/F_{380}$ = 0.14 ± 0.015, 0.30 ± 0.025, 0.25 ± 0.020 and 0.24 ± 0.025 in the G_1, S, G_2 and M phases, respectively; each value represents the average of the means (from 50 to 60 cells) of four independent experiments]. These results suggest that, although the absolute basal $[Ca^{2+}]_i$ level is not significantly different, the magnitude of basal Ca^{2+} influx is reduced during the G_1 phase of the cell cycle.

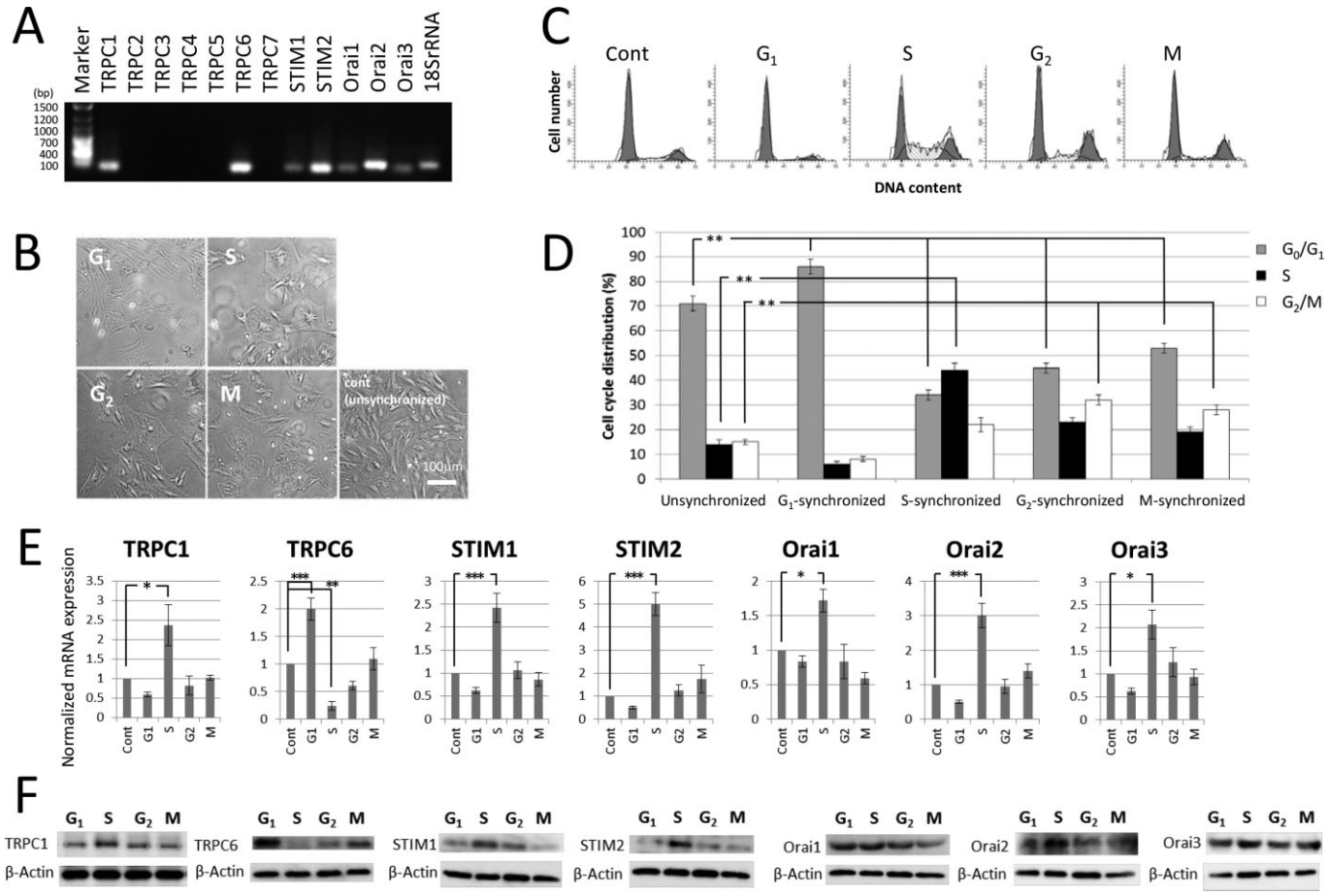

Figure 1

Cell cycle-dependent changes in the expression of TRPC1, TRPC6 and all subtypes of STIM and Orai in BMSCs. (A) mRNA expression profile of TRPC, STIM and Orai subtypes in non-synchronized BMSCs. Representative data of conventional PCR obtained from BMSC mRNAs extracted from seven rats. (B) phase-contrast images of cell cycle-synchronized BMSCs. Each cell cycle stage is labelled. The scale bar indicates 100 μm. All photographs were taken 4 days after drug application. Control (cont): non-synchronized cells. (C) representative histograms of cell cycle phase-synchronized BMSCs. All data were obtained 4 days after drug application. (D) Cell cycle distribution presented as % at different cell cycle stages evaluated by flow cytometry. Data are the averages of six experiments for each stage. **Significantly different from the control (unsynchronized) for each cell cycle stage ($P < 0.01$; Student's unpaired *t*-test). (E) mRNA expression levels of TRPC1, TRPC6, STIM and Orai at different stages of the cell cycle evaluated using real-time PCR analysis. In each graph, data are normalized to control (unsynchronized) and represent the mean of six independent experiments. *$P < 0.05$; **$P < 0.01$; ***$P < 0.001$, significantly different from the control; Student's unpaired *t*-test. (F) Western blot analysis of TRPC1, TRPC6, STIM and Orai at different cell cycle stages. Data are representative of six experiments.

RMP is deepest in the S phase

Up-regulation of SOCE-related molecules, such as TRPC1 and STIM/Orai (Figure 1E) and of SOCE (Figure 2A,B), during the S phase is suggestive of their roles for driving the cell cycle towards the S phase. However, the reciprocal decrease of TRPC6 expression in the same cell cycle phase is somewhat perplexing. It should, however, be noted that TRPC6 can predominantly permeate Na^+, being capable of positively shifting the RMP (Estacion *et al.*, 2006). In addition, in non-excitable cells, such as BMSCs, RMP has been reported to affect the transmembrane Ca^{2+} influx in such a way that depolarization decreases it (Gees *et al.*, 2010).

To explore the above possibility for BMSCs and to understand the role of RMP for cell cycle regulation more exactly, we systematically investigated the cell cycle dependence of RMP in BMSCs arrested at various stages of the cell cycle. As summarized in Figure 3A,B, the average RMP values were most negative in the S phase while least negative in the G_1 phase. These results are consistent with the cell cycle-dependent pattern of TRPC6 expression that was observed by PCR and immunoblot analyses (Figure 1E,F).

Although cell cycle synchronization procedures seemed effective to arrest BMSCs in the aimed phases, a minority of cells still remained unsychronized (Figure 1D), which may have introduced some errors in the evaluation. We therefore attempted to determine both cell cycle phases and RMPs in individual BMSCs using a cell cycle sensor FUCCI (Sakaue-Sawano *et al.*, 2008), without disturbing the cell cycle progression. As illustrated and demonstrated in Figure 3C,D respectively, FUCCI-expressing BMSCs showed red-, green- or yellow-coloured fluorescence depending on the cell cycle

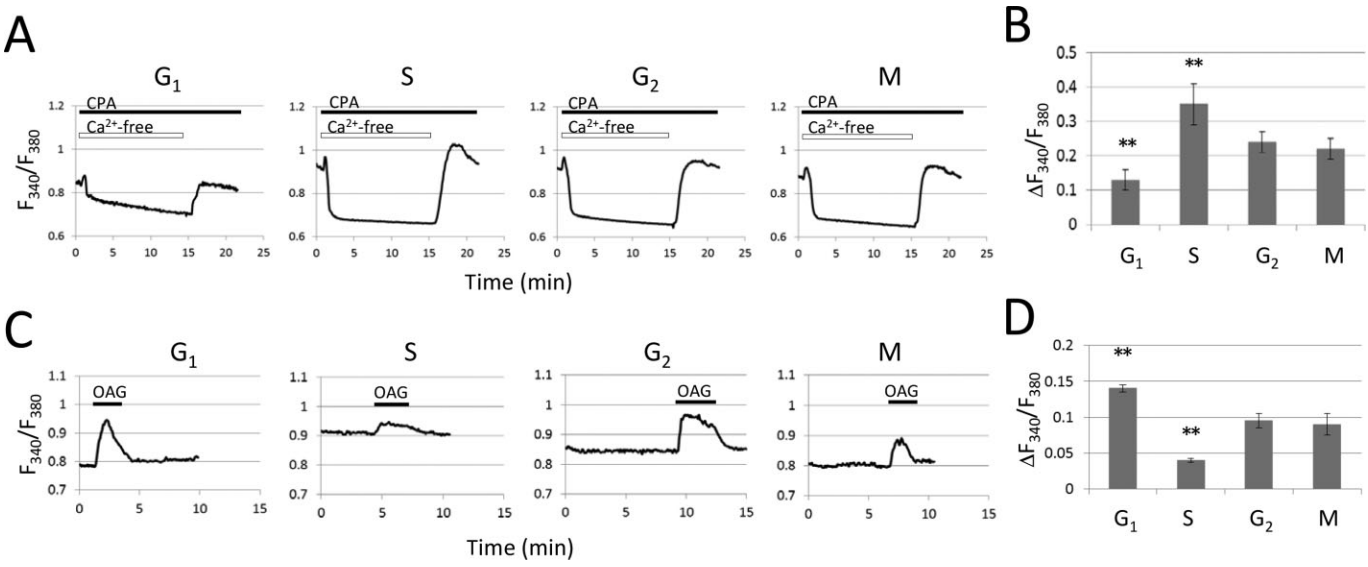

Figure 2

Store-operated (SOC) and OAG-evoked Ca^{2+} influxes in cell cycle-synchronized BMSCs. (A) Typical traces for SOCE at different stages of cell cycle. Cells were first depleted of stored Ca^{2+} by CPA (10 μM) in the absence of external Ca^{2+} and then re-exposed to 1.8 mM Ca^{2+}-containing external solution, which caused a large increase in $[Ca^{2+}]_i$. (B) The peaks of the SOC-mediated increases in $[Ca^{2+}]_i$ at different stages of cell cycle. Data are the averages of eight independent experiments (each represents the mean of 50–80 cells). **Statistically significant ($P < 0.01$) with ANOVA followed by Tukey–Kramer test. (C) Typical traces for OAG (100 μM)-evoked $[Ca^{2+}]_i$ increase at different cell cycle stages. (D) Magnitudes of OAG-evoked $[Ca^{2+}]_i$ increases at different cell cycle stages. Data are the averages of five independent experiments, each of which represents the mean of 50–70 cells. **Statistically significant ($P < 0.01$) with ANOVA followed by Tukey–Kramer test. Traces in panels A and C show the average time courses of $[Ca^{2+}]_i$ changes in more than 50 cells recorded on the same day.

phase in which they predominantly resided. The RMPs recorded from red-coloured BMSCs (–44.0 ± 1.1 mV; G_1 phase) were considerably less negative than those of green-coloured (–61.0 ± 2.9 mV; $S/G_2/M$ phase) or yellow-coloured (–58.0 ± 1.9 mV; G_1/S transition) BMSCs (Figure 3E). The relatively scattered RMP values in the $G_2/S/M$ phase (Figure 3F) may reflect the rather wide range of RMPs recorded from the three different cell cycle stages (i.e. S, G_2 and M). A similar tendency of reduced RMP in the G_1 phase was also observed by the nystatin-perforated current clamp recording [–52.8 ± 8 mV in the G_1 phase (red, $n = 21$), –67 ± 14 mV in the $S/G_2/M$ phase (green, $n = 7$), and –64.5 ± 12 mV in the G_1/S transition (yellow, $n = 7$)].

Combined with the results of Ca^{2+}-imaging and PCR/immunoblot analyses, these results collectively suggest that RMP is critical to determine the magnitude of SOCE during cell cycle progression (Figure 2B), to which the expression level of TRPC6 may substantially contribute (see succeeding sections).

Chemical clamping of RMP equalizes the magnitude of SOCE

To further corroborate the idea that RMP can itself alter the magnitude of SOCE in BMSCs, we employed two widely used membrane-depolarizing/hyperpolarizing manoeuvres.

As shown in Figure 4A, when bathed in a high K^+-solution, $DiBAC_4(3)$ fluorescence of BMSCs increased (i.e. depolarization occurred). It subsequently reached levels indistinguishable among different cell cycle stages. Similarly, bathing BMSCs in Na^+-free solution (Na^+ was substituted with NMDG), which decreased the $DiBAC_4(3)$ fluorescence (i.e. hyperpolarization occurred), also abolished the cell cycle-dependent differences in fluorescence (Figure 4A). Importantly, under these conditions, differences in the magnitude of SOCE observed among different cell cycle phases (Figure 2A,B) diminished almost completely, giving similarly decreased and increased magnitudes with depolarizing and hyperpolarizing procedures respectively (Figure 4B,C).

These results provide further compelling evidence that RMP itself is a crucial regulator for SOCE in BMSCs.

Knockdown of TRPC6 deepens the RMP and increases SOCE

To explore whether the expression level of TRPC6 causally regulates cell cycle-dependent changes in RMP and thereby the magnitude of SOCE in BMSCs, we assessed the effects of siRNA knockdown of TRPC6 on the RMP and SOCE with a voltage-sensitive fluorescent dye $DiBAC_4(3)$ and by the current clamp and Ca^{2+} imaging techniques. In preliminary experiments, we confirmed that TRPC6-targetting siRNA (siTRPC6) selectively inhibited TRPC6 expression (Supporting Information Figs. S1 and S2), as well as the response to OAG (Supporting Information Fig. S3).

$DiBAC_4(3)$ signals significantly decreased in siTRPC6-treated BMSCs; that is the RMP became hyperpolarized, as compared with those treated with control siRNA (siCon). In contrast, TRPC1-targetting siRNA (siTRPC1) was totally ineffective (Figure 5A). In current clamp experiments, siTRPC6

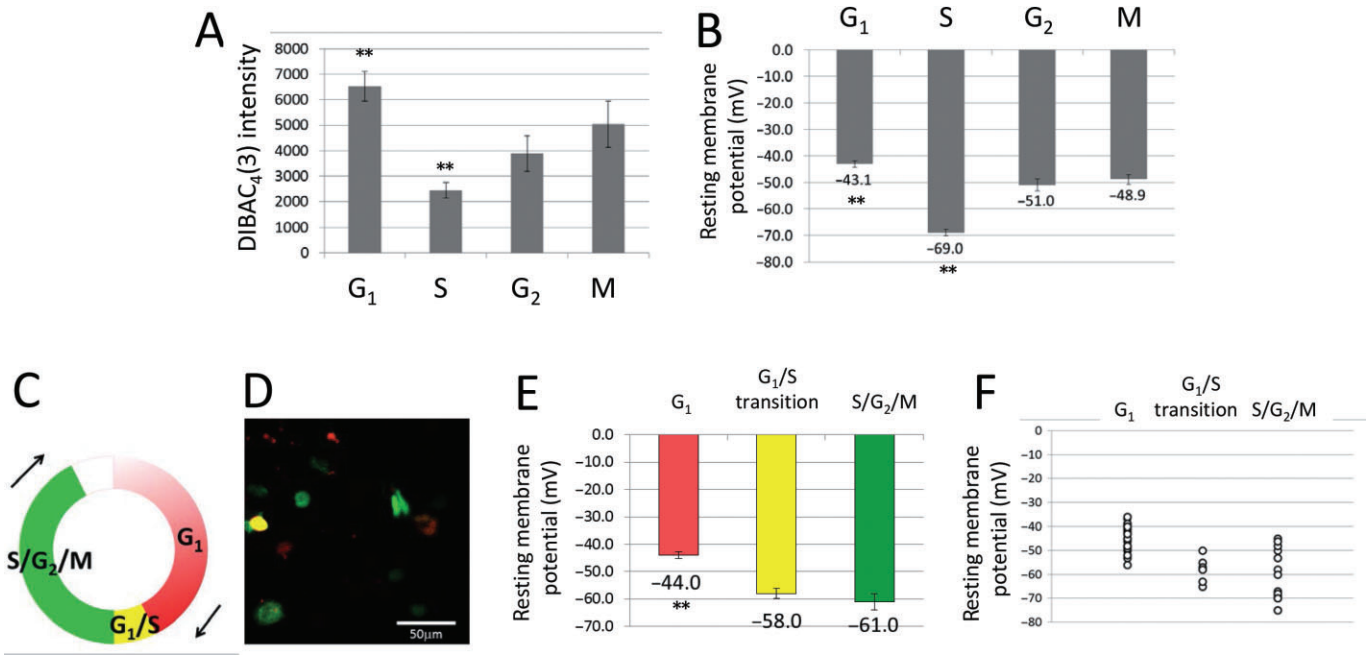

Figure 3

Cell cycle-dependent changes in the RMP of BMSC. (A) $DiBAC_4(3)$-based RMP measurements at different cell cycle phases. Columns represent the averages of data from six independent experiments, each of which represents the mean from 50–80 cells. **Statistically significant ($P < 0.01$) with ANOVA followed by Tukey–Kramer test. (B) RMP recorded using the current clamp method at different cell cycle phases. Data represent the average of 17 (G_1), 12 (S), 10 (G_2) and 15 (M) cells for each stage. **Significantly different among the four cell cycle stages ($P < 0.01$) with ANOVA followed by Tukey–Kramer test. (C) Schematic presentation of FUCCI-based, cell cycle-dependent colour changes. (D) Fluorescence image of FUCCI-expressing BMSCs. The scale bar indicates 50 μm. (E) Summary of FUCCI-based RMP measurements in BMSCs obtained by using current clamp recording. Columns represent averaged RMP values from 23 (G_1), 7 (G_1/S transition) and 14 (S/G_2/M) cells for each stage respectively. **Significantly different among the three stages ($P < 0.01$) with ANOVA with Steel–Dwass test. (F) Distribution of respective RMP values is shown in Figure 4E. Note that the FUCCI system cannot distinguish among the S/G_2/M phases.

treatment also caused a hyperpolarizing shift of RMP in BMSCs as compared with siTRPC1 or siCon treatment (–54.7 ± 1.8 mV in siTRPC6, –45.7 ± 2.4 mV in siTRPC1 and –43.1 ± 1.6 mV in control for siRNA; Figure 5B). Concomitantly, the magnitude of SOCE was significantly enhanced by siTRPC6 treatment (Figure 5C,D).

These results are consistent with the idea that, in the S phase, the RMP of BMSCs is maintained at a more hyperpolarized level than in the other phases via decreased basal TRPC6 activity, and that this hyperpolarized RMP level enhances the magnitude of SOCE by increasing the driving force for Ca^{2+} influx.

Knockdown of TRPC6 affects cell cycle progression and changes the expression pattern of cyclins

Finally, to more directly investigate the participation of TRPC6 channel in cell cycle progression of BMSCs, we analysed the effect of TRPC6 knockdown on cell cycle distribution, as well as the expression pattern of cyclins, key regulators of cell cycle progression (Coqueret, 2002). We performed cell cycle analyses at 4 days after siRNA treatment, when the expression of TRPC6 was selectively reduced (Supporting Information Figs. S1 and S2).

Table 1

Summary of the effects of TRPC6 knockdown on cell cycle progression

Culture condition	Cell cycle phase (%)		
	G_0/G_1	S	G_2/M
siCon	67.0 ± 4.0	11.0 ± 1.3	22.0 ± 2.0
siTRPC6	30.5 ± 2.9**	23.0 ± 2.0**	46.5 ± 1.8**

Values were taken from Figure 6B. siCon, negative control siRNA; siTRPC6, TRPC6-specific siRNA. Data represent the means ± SEM of six independent experiments. **Significantly different compared with siCon ($P < 0.01$, Student's unpaired *t*-test).

siRNA knockdown of TRPC6 dramatically changed the cell cycle distribution profile of BMSCs, with about twofold increases in the S and G_2/M phases (23.0% vs. 11.0% and 46.5% vs. 22.0% respectively; Figure 6B and Table 1). These changes were accompanied by the accumulation of cyclins A2 and B1, the major cyclins known to be up-regulated prior to G_1 phase entry (6.6- and 4.0-fold increases respectively; Figure 7).

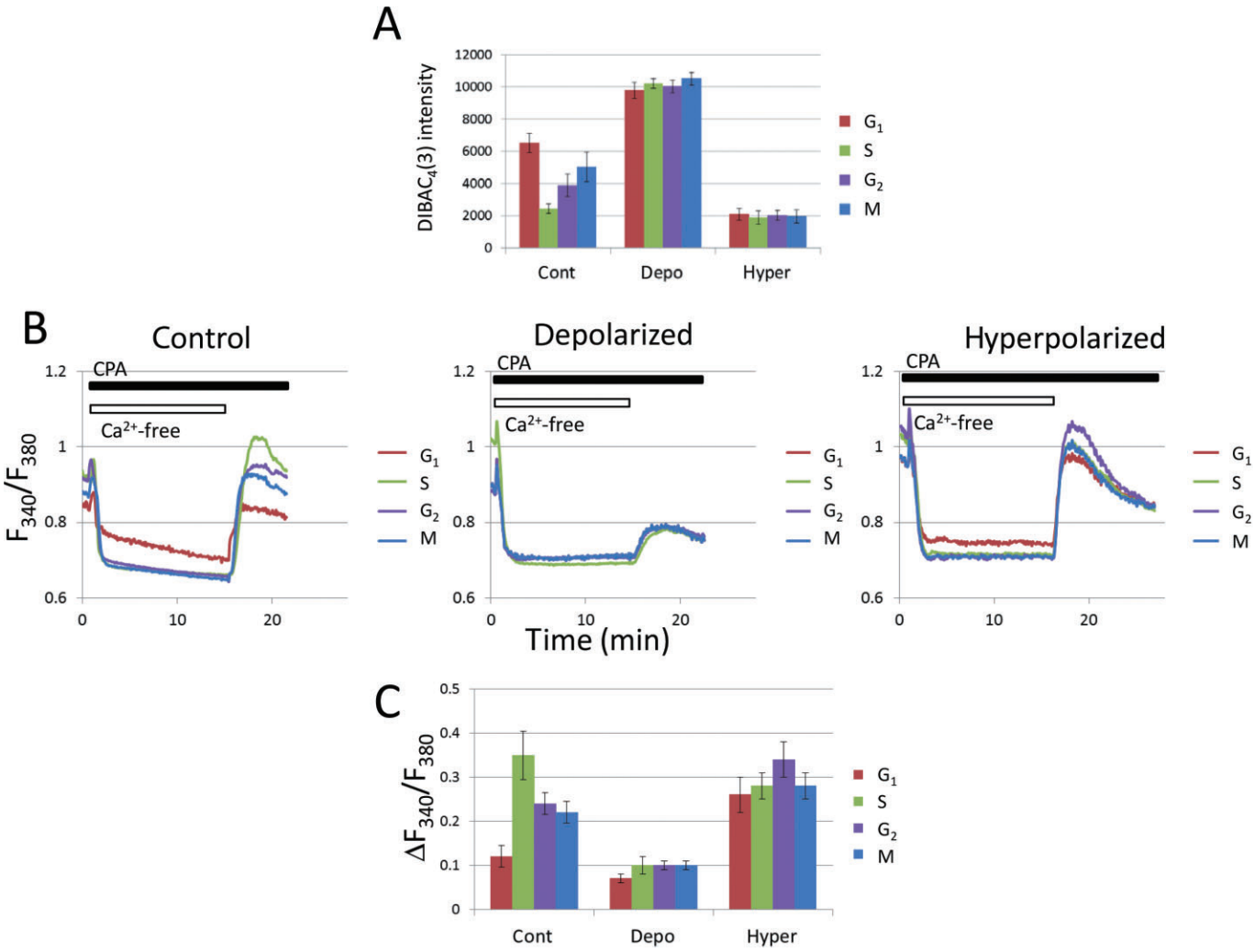

Figure 4

Excessive depolarization or hyperpolarization reduces the cell cycle-dependent differences in SOCE. (A) summary of RMP values at respective cell cycle stages under depolarized (by high extracellular K^+) or hyperpolarized (by replacing extracellular Na^+ to NMDG) conditions. Columns indicate the averages of six independent experiments (each represents the mean of 50–80 cells). Control is the same as shown in Figure 3A. (B) Actual records of SOCE for control (control), high-K^+ (depolarized) or Na^+-free (NMDG-substituted; hyperpolarized) conditions at different cell cycle stages. Traces show the averaged time courses from more than 50 cells obtained on the same day. Control traces are the same as shown in Figure 2A. (C) Summary of the peak magnitude of SOCE at respective cell cycle stages under control (*cont*), high-K^+ (*depo*) or Na^+-free (NMDG-substituted; *hyper*) conditions. Data for high-K^+ (*depo*) or Na^+-free (*hyper*) conditions are the averages of six independent experiments (each represents the mean of at least 50–80 cells). Data for control (*cont*) are the same as those shown in Figure 2B (averaged from eight independent experiments, each of which represents the mean of at least 50–80 cells).

These results strongly suggest that TRPC6 activity is essential for cell cycle progression during the G_1 phase in BMSCs.

Pharmacological inhibition of TRPC and SOC channels suppresses cell proliferation

In another series of experiments, we tested the effects of pharmacological inhibition of SOCE on BMSC proliferation. As there is no ideally specific inhibitor for SOC channel, we chose its representative inhibitor Gd^{3+} (1 μM). This concentration of Gd^{3+} has been reported to block SOCE with little effect on TRP channel activities (Trebak *et al.*, 2002). The application of Gd^{3+} at 1 μM did not affect RMP measured by either $DiBAC_4(3)$ fluorescence imaging or current clamp recording (data not shown). On the other hand, Gd^{3+} effectively slowed BMSC proliferation (Figure 8) and concomitantly suppressed store depletion-induced Ca^{2+} elevation (Supporting Information Fig. S4). Although circumstantial, these results indicate that cell cycle-dependent expression of STIM/Orai and the resultant changes in the magnitude of SOCE are not epiphenomena, but of primary importance for BMSC proliferation.

As for the role of TRPC6 channel in BMSC proliferation, we could not unequivocally test it because there is no known specific inhibitor for this channel. We, however, found that a reportedly TRPC-selective compound Pyr2 (Kiyonaka *et al.*,

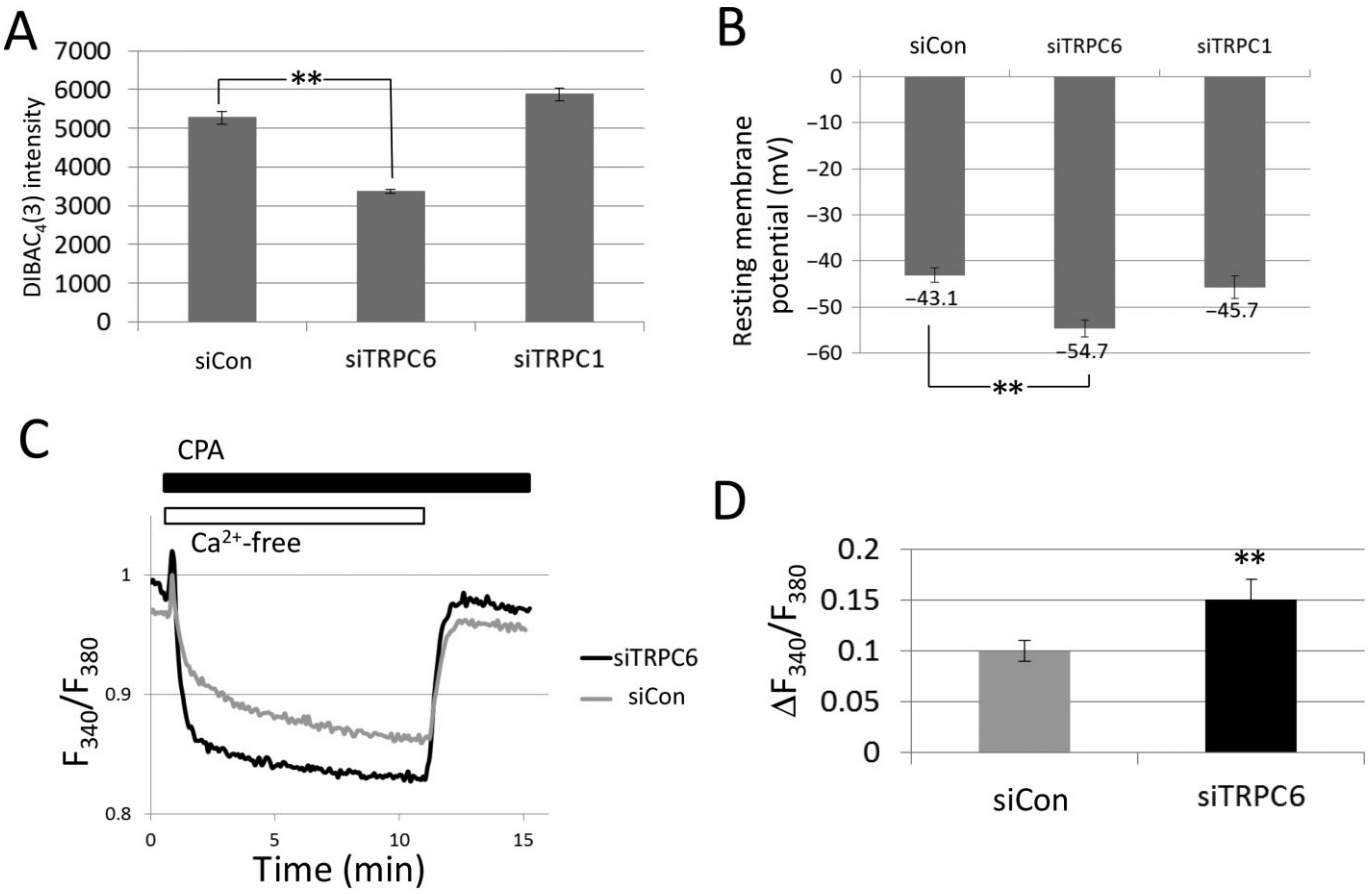

Figure 5

TRPC6 knockdown induces a negative shift in the membrane potential (RMP) and increases SOCE of BMSC. Experiments were performed 4 days after transfection with siRNA. siCon, control siRNA; siTRPC6, TRPC6-specific siRNA; siTRPC1, TRPC1-specific siRNA. (A) RMP was evaluated as a $DiBAC_4(3)$ fluorescence in siCon-, siTRPC6- and siTRPC1-treated BMSCs. Columns show the averaged RMP values from five independent experiments (each represents the mean of more than 60 cells). (B) Columns show the means of RMP recorded by the current clamp method, for siCon ($n = 10$), siTRPC6 ($n = 15$) and siTRPC1-treated ($n = 11$) BMSCs. (C) Typical traces of SOCE in siCon- and siTRPC6-treated cells. Each trace shows the averaged time course of at least 50 cells evaluated on the same day. (D) Summary of the magnitude of SOCE in siCon- or siTRPC6-treated cells. Data represent the averages of five independent experiments (each represents the mean of at least 50–70 cells). In panels A, B and D, the symbol '**' means significantly different from the control ($P < 0.01$); Student's unpaired *t*-test.

2009) also inhibited BMSC proliferation (Supporting Information Fig. S5), but this compound recently turned out to inhibit SOCE non-specifically (Schleifer *et al.*, 2012).

Discussion and conclusions

In this study, we found that the expression levels of TRPC1/C6 and SOCE-related molecules (STIM and Orai) in rat BMSCs vary in close linkage with the cell cycle. The mRNA and protein expression levels of STIM/Orai and TRPC1 were high in the S phase, whereas those of TRPC6 were low in the same cell cycle phase. Many previous studies in other cell types including both normal and cancer cells reported that expressions of TRPC subtypes and STIM/Orai are correlated with cell cycle progression (Abdullaev *et al.*, 2008; Cai *et al.*, 2009; Potier *et al.*, 2009; Ding *et al.*, 2010; Leuner *et al.*, 2011; Li *et al.*, 2012; Tajeddine and Gailly, 2012). However, these studies focused mostly on the cell cycle-arresting effects of TRPC or STIM/Orai knockdown, and did not examine their expression profiles over the whole-cell cycle. In this respect, the present study is the first detailed investigation of cell cycle-dependent changes in TRPC and STIM/Orai expression, in conjunction with associated functions such as SOC activity, membrane potential and cell cycle progression.

Our results indicate that SOC activity in BMSCs is highest in the S phase and lowest in the G_1 phase. This is paralleled by altered expression of the SOCE-related molecules, TRPC1, Orai and STIM. It is known that an elevated $[Ca^{2+}]_i$ level is a requisite to drive the cell cycle, and that sustained Ca^{2+} influx through SOC activates the calcineurin-NFAT (nuclear factor of activated T-cells) pathway thereby promoting the proliferation of T lymphocytes and vascular smooth muscle cells (Lipskaia and Lompré, 2004; Kotturi *et al.*, 2006; Gwack *et al.*, 2007). Activation of NFAT signalling was also found to be essential for the undifferentiation of BMSCs (Kawano *et al.*,

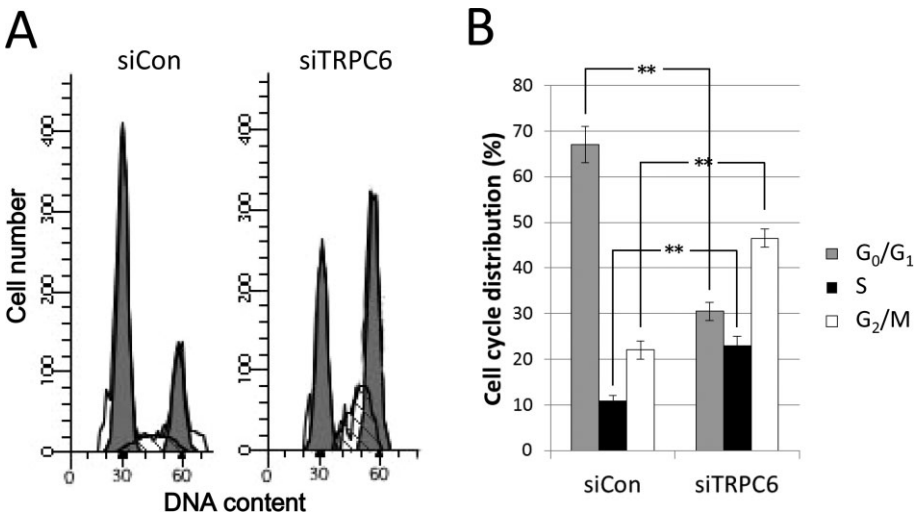

Figure 6

Effect of TRPC6 knockdown on BMSC cell cycle progression. Experiments were performed 4 days after transfection with siRNA. siCon, negative control siRNA; siTRPC6, siRNA specifically targeting TRPC6. (A) Cell cycle distribution of siCon- and siTRPC6-transfected BMSCs. Data are representative of six experiments. (B) Average percentages of cells residing in respective cell cycle stages for each siRNA treatment (n = 6 respectively). **Statistically significant ($P < 0.01$); Student's unpaired t-test.

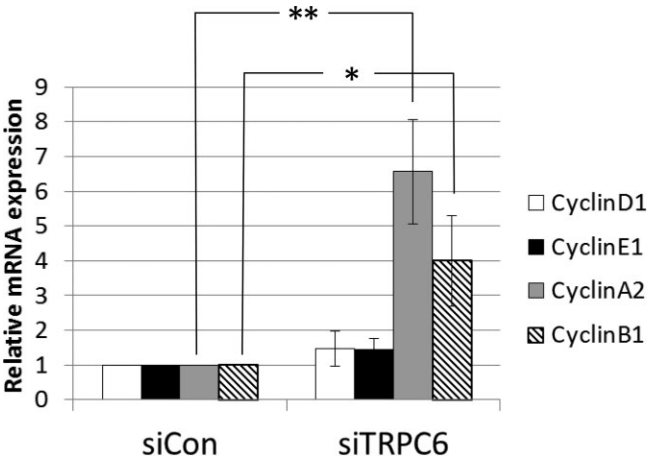

Figure 7

Cyclin mRNA expression profile after knockdown of TRPC6. Experiments were performed 4 days after transfection with siRNA. siCon, negative control siRNA. Each column in the right panel (siTRPC6) represents a value relative to the corresponding control (siCon); data are the average of six independent experiments. *$P < 0.05$ and **$P < 0.01$, Student's unpaired t-test. Information on specific primers is given in Supporting Information Table S1.

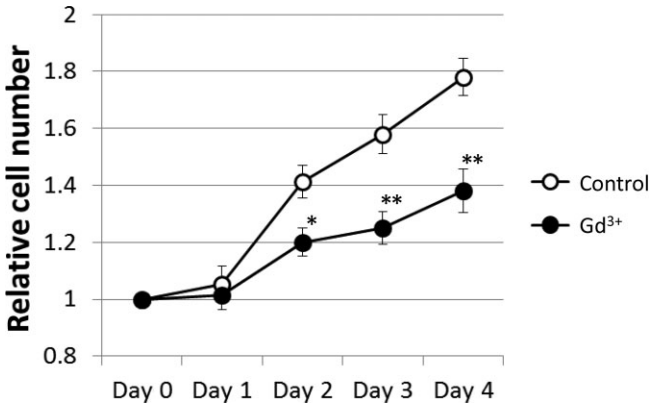

Figure 8

The effect of Gd^{3+} (1 μM) on BMSC proliferation. Each data point is normalized to the corresponding one on day 0 for each condition and represents the average of five independent experiments. *$P < 0.05$ and **$P < 0.01$, significantly different from the control; Student's unpaired t-test.

2006). It is thus plausible that a similar NFAT-dependent mechanism may be involved in Ca^{2+}-mediated regulation of BMSC proliferation.

In principle, SOC activity can be controlled not only by altered membrane expression of SOCE-related molecules via transcription, translation, trafficking and degradation processes, but also by any other post-translational mechanisms that can alter the functionality of these molecules. For instance, Smyth *et al.* (2009) reported that phosphorylation of STIM1 at Ser^{486} and Ser^{668} controls the translocation of STIM1 to the plasma membrane, resulting in decreased SOC activity in the M phase (Smyth *et al.*, 2009). As will be discussed in the following section, our present findings also suggest that membrane potential is a key regulator of SOC activity in BMSCs, in which TRPC6 plays a particular role.

Membrane potential modulated by TRPC6 may be a key mechanism regulating SOC activity of BMSCs

The RMP of BMSCs showed cell cycle-dependent changes, being most depolarized in the G_1 phase and hyperpolarized in

the S phase (Figure 3). This cell cycle-dependent profile of RMP exactly matches the observed G_1 phase up-regulation and S phase down-regulation of TRPC6 (Figure 1E,F) and with the fact that knockdown of TRPC6 reduces the RMP (Figure 5). These observations give rise to the idea that the cell cycle progression of BMSCs may be tightly regulated by TRPC6 channel activity through changes in the RMP. In general, members of the TRPC subfamily including TRPC6 are recognized as Ca^{2+} entry channels. However, poor cation discrimination makes them act as 'depolarization channels' that pass Na^+ inwardly across the cell membrane (Estacion *et al.*, 2006). This means that activation of TRPC channels can lead to membrane depolarization (Soboloff *et al.*, 2005) reducing the driving force for Ca^{2+} influx through any non-voltage-gated Ca^{2+} entry pathways such as SOC channels (Gees *et al.*, 2010).

This scenario indeed appears applicable for TRPC6 channels for the following reasons. Firstly, SOCE was lowest in the G_1 phase and highest in the S phase whereas TRPC6 expression was highest and lowest in these phases respectively (Figure 2A). Secondly, artificial depolarization/hyperpolarization manoeuvres suppressed/enhanced SOCE and reduced the differences in the magnitude of SOCE among the cell cycle stages (Figure 4). Thirdly, SOCE was increased by siTRPC6 which simultaneously caused a negative shift in RMP (Figure 5). Finally, despite the decreased SOCE in the G_1 phase (Figure 2A,B), the mRNA levels of TRPC1 and STIM/Orai were not dramatically decreased at the same cell cycle stage (Figure 1E). This last finding further suggests the critical role of TRPC6 in regulating SOCE in BMSCs. However, there is a caveat against the interpretation of TRPC6 knockdown data, as it is still uncertain whether it was the decreased TRPC6 expression or the consequent alteration in cell cycle distribution (i.e. decreased population of BMSCs in the G_1 phase; Figure 6) that ultimately was responsible for the observed negative shift in the RMP. Acute and selective inhibition of TRPC6 channel activity, for example by its specific blocker, may unequivocally distinguish between these possibilities.

In addition, although no significant changes in the basal $[Ca^{2+}]_i$ level were detected among different cell cycle stages, the magnitude of basal Ca^{2+} influx assessed by external Ca^{2+} removal was clearly reduced during the G_1 phase (see the Results section). This could also be accounted for by the up-regulation of TRPC6 channel which would reduce the RMP (i.e. depolarizes the membrane more) thereby decreasing the driving force for basal Ca^{2+} influx. Conceivably, the decreased basal Ca^{2+} influx might then reduce stored Ca^{2+} content and attenuate the subsequent SOCE. Although the molecular entity of basal Ca^{2+} influx pathway remains to be determined, these results support pivotal roles of TRPC6 channel for regulating both unstimulated and stimulated (by store-depleting stimuli) Ca^{2+} influxes and thereby BMSC proliferation via membrane depolarization-mediated mechanisms.

A similar mechanism involving TRP channels in regulating RMP, SOCE and cellular function has also been reported for bone marrow-derived mast cells. Therein, knockout of TRPM4 expression enhanced the driving force for IgE-induced Ca^{2+} entry and thereby facilitated the release of inflammatory mediators, histamine, leukotrienes and tumour necrosis factor (Vennekens *et al.*, 2007). Interestingly, in our preliminary experiments, TRPM5, another BMSC-abundant TRP isoform and the closest homologue of TRPM4, also showed a cell cycle-dependent expression pattern similar to that of TRPC6 (J. Ichikawa and R. Inoue, unpubl. data). Thus, RMP-mediated regulation of Ca^{2+} entry via altered TRP channel activities may be a widely operating mechanism to modulate the functions of non-excitable cells such as BMSCs.

TRPC6 may control cell cycle progression by regulating the levels of cyclins

Our siRNA experiments showed that elimination of TRPC6 greatly affected cell cycle progression with a twofold increase in the BMSC populations in the S and G_2/M phases and reducing the number in the G_0/G_1 phase by half (Figure 6 and Table 1). This pattern was similar to those observed under S-, G_2- or M-arrested conditions (Figure 1), and is consistent with the notable accumulation of the S/G_2/M-specific cyclins A2 and B1 (Coqueret, 2002) observed upon TRPC6 knockdown (Figure 7). Cyclins play an important role in driving the cell cycle in conjunction with cyclin-dependent kinases (CDKs). The periodic synthesis and degradation of four cyclins (cyclin A, B, D and E) phosphorylate CDKs at appropriate timings in a cell cycle-specific manner (Coqueret, 2002). Thus, although the mechanism involved remains unclear, the above findings may suggest that cell cycle-specific changes in TRPC6 channel activity, by altering cyclin levels, are essential for the transition from the S/G_2/M to G_0/G_1 phases. How this mechanism involves RMP-regulated SOC activity will need further investigation.

Membrane potential may have more ubiquitous roles in the regulation of long-term cellular functions

In several types of cells, there is good evidence suggesting that RMP plays non-trivial roles in regulating cell differentiation/undifferentiation/proliferation processes. It is generally thought that the depolarized state enhances DNA synthesis and cell cycle progression, while the hyperpolarized state drives cells into differentiation. For example, it has been reported that hyperpolarization stops the proliferation of endothelial cells, with accompanying down-regulation of cyclin E and up-regulation of a cyclin inhibitor p27 (Wang *et al.*, 2003). Conversely, depolarization has been shown to promote DNA synthesis in macrophages (Kong *et al.*, 1991). Even in mature neurons in which differentiation is terminated, prolonged depolarization leads to mitosis and DNA synthesis (Stillwell *et al.*, 1973; Cone and Cone, 1976). The level of RMP also significantly affects the differentiation potential of BMSCs. Differentiation of BMSCs into osteoblasts or adipocytes is accompanied by membrane hyperpolarization, and conversely, culturing undifferentiated BMSCs under depolarized conditions prevents their differentiation while hyperpolarizing reagents facilitate osteogenic differentiation (Sundelacruz *et al.*, 2008). These findings again suggest that changes in RMP, by altering the function of ion channels, may strongly influence the phenotypic transformation of cells among differentiation, undifferentiation and proliferation through cell cycle regulation.

In human MSCs, a high extracellular glucose level induces phosphorylation of PKC, MAPK and activation of the PI3K-Akt pathway which leads to the synthesis of cyclin D/E (Ryu *et al.*, 2010). The PI3K-Akt pathway is known to be activated by electrical stimulation (Zhao *et al.*, 2006). Changes in membrane potential may also activate PI3K and enhance the cyclin D/E synthesis of BMSCs. Consistently, we confirmed the inhibitory effect of TRPC6 knockdown on the phosphorylation of Akt, but this was not observed for the expression of cyclin D1 protein (Supporting Information Fig. S6; note also that cyclin D1 mRNA level was not changed by TRPC6 knockdown; see Figure 7). Further thorough studies are needed to determine in what way TRPC6 activity regulates the PI3K-Akt signalling pathway.

Membrane potential is also known to modulate the agonist-binding affinity of the M_2 muscarinic receptor (Ben-Chaim *et al.*, 2006) and IP_3 production pathway (Billups *et al.*, 2006). Provided that such modulation of metabotropic receptors by membrane potential would be operative in BMSCs, cell cycle-dependent changes in RMP may variably affect both receptor- and store-operated Ca^{2+} mobilizing mechanisms and this may lead to further complex consequences.

Limitations of the present study

There are a number of technical limitations, which results in some uncertainties in our conclusions. Firstly, the pharmacological interventions we used failed to arrest BMSCs exactly at the desired cell cycle stages (see Figure 1C,D). Even with an alternative approach using the FUCCI cell cycle sensor, we could only distinguish among the G_1 phase, G_1/S boundary and S/G_2/M phases. Thus, although statistically significant, the observed differences in RMP and TRPC6 expression levels between the S and non-S phases will require further rigorous scrutiny with better tools/strategies that can separate four cell cycle stages more exactly. Secondly, the relatively low transfection efficiency of siRNAs in primary cultured BMSCs did not completely suppress the expression of targeted TRPC proteins including TRPC6 and TRPC1. One promising alternative to the siRNA technology is knockout animals. In fact, there are several knockout mice deficient in the *trpc* genes available. However, this approach is unlikely to be suitable for the purpose of the present study for the following reasons. The profile of TRPC subtype expression varies considerably among different species of animals and/or the different strains of the same animal species. For example, BMSCs from F344 rats (which were used in the present study) express TRPC6 but not TRPC3, while those from Wistar rats express both. Such differences could be more serious between different species such as rats and mice, and only the latter has TRP knockout models available. Another issue is that, even in TRP-knockout animals, a compensatory up-regulation of homologous TRP isoforms may obscure the functional deficiency. In fact, it was previously shown that, in a TRPC6-knockout mouse, its closest homologue TRPC3 was up-regulated and caused a functional overcompensation (Dietrich *et al.*, 2005; Sel *et al.*, 2008). Nonetheless, we did not observe such compensatory up-regulation in F344 BMSCs subchronically treated with cell cycle-synchronizing agents or siRNA. We would also like to point out that, although TRPC6's mRNA level of BMSCs was decreased only to ~50% by siRNA treatment (Supporting Information Fig. S1), its protein level was more substantially decreased (Supporting Information Fig. S2, we used siTRPC6 cells at day 4 for our study). Thus, we believe that our present data tolerably reflect TRPC6-deficient conditions, but this issue needs further clarification.

In summary, the present study has provided the first clear evidence that the activities of TRPC/SOCE-related molecules are closely correlated with the cell cycle progression of BMSCs. In particular, the role of TRPC6 therein seems unique in that its altered expression during the cell cycle effectively changes the RMP and affects SOCE and cell cycle progression/proliferation (Figure 9). Until now, such a tight functional link between the cell cycle and electrical properties has not received enough attention in regenerative medicine or in investigations into the physiology/pathophysiology of stem cells including BMSCs (Sundelacruz *et al.*, 2009). In this respect, the present findings may serve to develop a novel therapeutic strategy for modulating the proliferative/phenotypic plasticity of these cells. Further studies to assess the significance of targeting TRPC6 with its specific blockers or TRPC6-knockout animals are warranted.

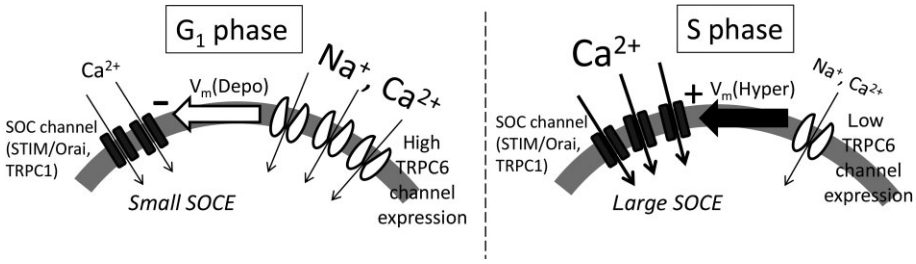

Figure 9

Schematic diagram of the role of the TRPC6 channel in cell cycle progression of BMSCs. In the G_1 phase, the highest expression level of TRPC6 induces membrane depolarization (*Depo*) and functionally suppresses Ca^{2+} entry via SOC channels (indicated by '–') in BMSCs. On the contrary, the lowest expression level of TRPC6 in the S phase maintains RMP at a more hyperpolarized level (*Hyper*) and enhances SOC-mediated Ca^{2+} entry (indicated by '+'). The highest expression levels of STIM/Orai and TRPC1 molecules in the S phase also contribute to an enhanced SOCE. V_m, membrane potential.

Acknowledgements

We thank Professor Yasuo Mori (Kyoto University) for providing us with Pyr2 compound. This work was supported by a Grant-in-Aid to J. I. from The Clinical Research Promotion Foundation.

Author contributions

J. I. was responsible for the conception and design of the experiments. J. I. performed experiments and analysed data. R. I. helped with some of experimental design and commented on the manuscript. J. I. and R. I. discussed the results, J. I. drafted the paper and R. I. commented on the manuscript. All authors approved the final version of the manuscript.

Conflict of interest

The authors declare no conflict of interest.

References

Abdullaev IF, Bisaillon JM, Potier M, Gonzalez JC, Motiani RK, Trebak M (2008). Stim1 and Orai1 mediate CRAC currents and store-operated calcium entry important for endothelial cell proliferation. Circ Res 103: 1289–1299.

Alexander SPH, Benson HE, Faccenda E, Pawson AJ, Sharman JL, Spedding M *et al.* (2013a). The Concise Guide to PHARMACOLOGY 2013/14: G protein-coupled receptors. Br J Pharmacol 170: 1459–1581.

Alexander SPH, Benson HE, Faccenda E, Pawson AJ, Sharman JL, Spedding M *et al.* (2013b). The Concise Guide to PHARMACOLOGY 2013/14: Ion channels. Br J Pharmacol 170: 1607–1651.

Alexander SPH, Benson HE, Faccenda E, Pawson AJ, Sharman JL, Spedding M *et al.* (2013c). The Concise Guide to PHARMACOLOGY 2013/14: Enzymes. Br J Pharmacol 170: 1797–1867.

Armisén R, Marcelain K, Simon F, Tapia JC, Toro J, Quest AF *et al.* (2011). TRPM4 enhances cell proliferation through up-regulation of the β-catenin signaling pathway. J Cell Physiol 226: 103–109.

Becchetti A (2011). Ion channels and transporters in cancer. 1. Ion channels and cell proliferation in cancer. Am J Physiol Cell Physiol 301: C255–C265.

Beech DJ (2007). Ion channel switching and activation in smooth-muscle cells of occlusive vascular diseases. Biochem Soc Trans 35: 890–894.

Ben-Chaim Y, Chanda B, Dascal N, Bezanilla F, Parnas I, Parnas H (2006). Movement of 'gating charge' is coupled to ligand binding in a G-protein-coupled receptor. Nature 444: 106–109.

Berridge MJ, Bootman MD, Roderick HL (2003). Calcium signalling: dynamics, homeostasis and remodelling. Nat Rev Mol Cell Biol 4: 517–529.

Billups D, Billups B, Challiss RA, Nahorski SR (2006). Modulation of Gq-protein-coupled inositol trisphosphate and Ca^{2+} signaling by the membrane potential. J Neurosci 26: 9983–9995.

Cahalan MD (2009). STIMulating store-operated Ca^{2+} entry. Nat Cell Biol 11: 669–677.

Cai R, Ding X, Zhou K, Shi Y, Ge R, Ren G *et al.* (2009). Blockade of TRPC6 channels induced G_2/M phase arrest and suppressed growth in human gastric cancer cells. Int J Cancer 125: 2281–2287.

Caplan AI (2007). Adult mesenchymal stem cells for tissue engineering versus regenerative medicine. J Cell Physiol 213: 341–347.

Cheng H, Feng JM, Figueiredo ML, Zhang H, Nelson PL, Marigo V *et al.* (2010). Transient receptor potential melastatin type 7 channel is critical for the survival of bone marrow derived mesenchymal stem cells. Stem Cells Dev 19: 1393–1403.

Cone CD, Cone CM (1976). Induction of mitosis in mature neurons in central nervous system by sustained depolarization. Science 192: 155–158.

Coqueret O (2002). Linking cyclins to transcriptional control. Gene 299: 35–55.

Dhennin-Duthille I, Gautier M, Faouzi M, Guilbert A, Brevet M, Vaudry D *et al.* (2011). High expression of transient receptor potential channels in human breast cancer epithelial cells and tissues: correlation with pathological parameters. Cell Physiol Biochem 28: 813–822.

Dietrich A, Schnitzler MM, Gollasch M, Gross V, Storch U, Dubrovska G *et al.* (2005). Increased vascular smooth muscle contractility in $TRPC6^{-/-}$ mice. Mol Cell Biol 25: 6980–6989.

Ding X, He Z, Zhou K, Cheng J, Yao H, Lu D *et al.* (2010). Essential role of TRPC6 channels in G_2/M phase transition and development of human glioma. J Natl Cancer Inst 102: 1052–1068.

El Boustany C, Katsogiannou M, Delcourt P, Dewailly E, Prevarskaya N, Borowiec AS *et al.* (2010). Differential roles of STIM1, STIM2 and Orai1 in the control of cell proliferation and SOCE amplitude in HEK293 cells. Cell Calcium 47: 350–359.

Elliott AC (2001). Recent developments in non-excitable cell calcium entry. Cell Calcium 30: 73–93.

Estacion M, Sinkins WG, Jones SW, Applegate MAB, Schilling WP (2006). Human TRPC6 expressed in HEK 293 cells forms non-selective cation channels with limited Ca^{2+} permeability. J Physiol 572: 359–377.

Gees M, Colsoul B, Nilius B (2010). The role of transient receptor potential cation channels in Ca^{2+} signaling. Cold Spring Harb Perspect Biol 2: a003962.

Gwack Y, Feske S, Srikanth S, Hogan PG, Rao A (2007). Signalling to transcription: store-operated Ca^{2+} entry and NFAT activation in lymphocytes. Cell Calcium 42: 145–156.

Hofmann T, Obukhov AG, Schaefer M, Harteneck C, Gudermann T, Schultz G (1999). Direct activation of human TRPC6 and TRPC3 channels by diacylglycerol. Nature 397: 259–263.

Ichikawa J, Gemba H (2009). Cell density-dependent changes in intracellular Ca^{2+} mobilization via the $P2Y_2$ receptor in rat bone marrow stromal cells. J Cell Physiol 219: 372–381.

Kawano S, Otsu K, Kuruma A, Shoji S, Yanagida E, Muto Y *et al.* (2006). ATP autocrine/paracrine signaling induces calcium oscillations and NFAT activation in human mesenchymal stem cells. Cell Calcium 39: 313–324.

Kiyonaka S, Kato K, Nishida M, Mio K, Numaga T, Sawaguchi Y *et al.* (2009). Selective and direct inhibition of TRPC3 channels underlies biological activities of a pyrazole compound. Proc Natl Acad Sci U S A 106: 5400–5405.

Kong SK, Suen YK, Choy YM, Fung KP, Lee CY (1991). Membrane depolarization was required to induce DNA synthesis in murine macrophage cell line PU5-1.8. Immunopharmacol Immunotoxicol 13: 329–339.

Kotturi MF, Hunt SV, Jefferies WA (2006). Roles of CRAC and Cav-like channels in T cells: more than one gatekeeper? Trends Pharmacol Sci 27: 360–367.

Krebsbach PH, Kuznetsov SA, Bianco P, Robey PG (1999). Bone marrow stromal cells: characterization and clinical application. Crit Rev Oral Biol Med 10: 165–181.

Leuner K, Kraus M, Woelfle U, Beschmann H, Harteneck C, Boehncke WH *et al.* (2011). Reduced TRPC channel expression in psoriatic keratinocytes is associated with impaired differentiation and enhanced proliferation. PLoS ONE 6: e14716.

Li M, Chen C, Zhou Z, Xu S, Yu Z (2012). A TRPC1-mediated increase in store-operated Ca^{2+} entry is required for the proliferation of adult hippocampal neural progenitor cells. Cell Calcium 51: 486–496.

Lipskaia L, Lompré AM (2004). Alteration in temporal kinetics of Ca^{2+} signaling and control of growth and proliferation. Biol Cell 96: 55–68.

Nilius B, Owsianik G, Voets T, Peters JA (2007). Transient receptor potential cation channels in disease. Physiol Rev 87: 165–217.

Oguri A, Tanaka T, Iida H, Meguro K, Takano H, Oonuma H *et al.* (2010). Involvement of CaV3.1 T-type calcium channels in cell proliferation in mouse preadipocytes. Am J Physiol Cell Physiol 298: C1414–C1423.

Parekh AB (2007). Functional consequences of activating store-operated CRAC channels. Cell Calcium 42: 111–121.

Pawson AJ, Sharman JL, Benson HE, Faccenda E, Alexander SP, Buneman OP *et al.*; NC-IUPHAR (2014). The IUPHAR/BPS Guide to PHARMACOLOGY: an expert-driven knowledgebase of drug targets and their ligands. Nucl Acids Res 42 (Database Issue): D1098–106.

Pittenger MF, Mackay AM, Beck SC, Jaiswal RK, Douglas R, Mosca JD *et al.* (1999). Multilineage potential of adult human mesenchymal stem cells. Science 284: 143–147.

Potier M, Trebak M (2008). New developments in the signaling mechanisms of the store-operated calcium entry pathway. Pflugers Arch 457: 405–415.

Potier M, Gonzalez JC, Motiani RK, Abdullaev IF, Bisaillon JM, Singer HA *et al.* (2009). Evidence for STIM1- and Orai1-dependent store-operated calcium influx through I_{CRAC} in vascular smooth muscle cells: role in proliferation and migration. FASEB J 23: 2425–2437.

Pricola KL, Kuhn NZ, Haleem-Smith H, Song Y, Tuan RS (2009). Interleukin-6 maintains bone marrow-derived mesenchymal stem cell stemness by an ERK1/2-dependent mechanism. J Cell Biochem 108: 577–588.

Prockop DJ (1997). Marrow stromal cells as stem cells for nonhematopoietic tissues. Science 276: 71–74.

Ryu JM, Lee MY, Yun SP, Han HJ (2010). High glucose regulates cyclin D1/E of human mesenchymal stem cells through TGF-β_1 expression via Ca^{2+}/PKC/MAPKs and PI3K/Akt/mTOR signal pathways. J Cell Physiol 224: 59–70.

Sakaue-Sawano A, Kurokawa H, Morimura T, Hanyu A, Hama H, Osawa H *et al.* (2008). Visualizing spatiotemporal dynamics of multicellular cell-cycle progression. Cell 132: 487–498.

Schleifer H, Doleschal B, Lichtenegger M, Oppenrieder R, Derler I, Frischauf I *et al.* (2012). Novel pyrazole compounds for pharmacological discrimination between receptor-operated and store-operated Ca^{2+} entry pathways. Br J Pharmacol 167: 1712–1722.

Sel S, Rost BR, Yildirim AO, Sel B, Kalwa H, Fehrenbach H *et al.* (2008). Loss of classical transient receptor potential 6 channel reduces allergic airway response. Clin Exp Allergy 38: 1548–1558.

Smyth JT, Petranka JG, Boyles RR, DeHaven WI, Fukushima M, Johnson KL *et al.* (2009). Phosphorylation of STIM1 underlies suppression of store-operated calcium entry during mitosis. Nat Cell Biol 11: 1465–1472.

Soboloff J, Spassova M, Xu W, He L, Cuesta N, Gill DL (2005). Role of endogenous TRPC6 channels in Ca^{2+} signal generation in A7r5 smooth muscle cells. J Biol Chem 280: 39786–39794.

Stillwell EF, Cone CM, Cone CD (1973). Stimulation of DNA synthesis in CNS neurones by sustained depolarisation. Nat New Biol 246: 110–111.

Sundelacruz S, Levin M, Kaplan DL (2008). Membrane potential controls adipogenic and osteogenic differentiation of mesenchymal stem cells. PLoS ONE 3: e3737.

Sundelacruz S, Levin M, Kaplan DL (2009). Role of membrane potential in the regulation of cell proliferation and differentiation. Stem Cell Rev 5: 231–246.

Tajeddine N, Gailly P (2012). TRPC1 protein channel is major regulator of epidermal growth factor receptor signaling. J Biol Chem 287: 16146–16157.

Trebak M, Bird GS, McKay RR, Putney JW (2002). Comparison of human TRPC3 channels in receptor-activated and store-operated modes. Differential sensitivity to channel blockers suggests fundamental differences in channel composition. J Biol Chem 277: 21617–21623.

Uccelli A, Moretta L, Pistoia V (2008). Mesenchymal stem cells in health and disease. Nat Rev Immunol 8: 726–736.

Vaca L (2010). SOCIC: the store-operated calcium influx complex. Cell Calcium 47: 199–209.

Vennekens R, Olausson J, Meissner M, Bloch W, Mathar I, Philipp SE *et al.* (2007). Increased IgE-dependent mast cell activation and anaphylactic responses in mice lacking the calcium-activated nonselective cation channel TRPM4. Nat Immunol 8: 312–320.

Wang E, Yin Y, Zhao M, Forrester JV, McCaig CD (2003). Physiological electric fields control the G_1/S phase cell cycle checkpoint to inhibit endothelial cell proliferation. FASEB J 17: 458–460.

Zhao M, Song B, Pu J, Wada T, Reid B, Tai G *et al.* (2006). Electrical signals control wound healing through phosphatidylinositol-3-OH kinase-gamma and PTEN. Nature 442: 457–460.

Supporting information

Additional Supporting Information may be found in the online version of this article at the publisher's web-site:

http://dx.doi.org/10.1111/bph.12840

Figure S1 Quantitative real-time PCR analysis with siRNAs specific for TRPC1 and TRPC6. Target specificity of each siRNA is demonstrated. siCon, negative control siRNA;

siTRPC1, TRPC1-specific siRNA; siTRPC6, TRPC6-specific siRNA. Experiments were performed 4 days after transfection with siRNA. Data represent the average of five independent experiments and are normalized to those of siCon. **Significantly different to siCon ($P < 0.01$, Student's unpaired *t*-test).

Figure S2 Effects of siRNA knockdown on TRPC1 or TRPC6 protein levels. siCon, siTRPC1 and siTRPC6: the same abbreviations as in Supporting Information Fig. S1. After siRNA treatment for at least 3 days, the expression of both proteins was almost completely lost. Data are representative of five independent experiments.

Figure S3 The effect of TRPC6 siRNA treatment on OAG-induced Ca^{2+} response. siCon and siTRPC6: the same abbreviations as in Supporting Information Fig. S1. Experiments were performed 4 days after transfection with siRNA. Knockdown of TRPC6 significantly decreased $[Ca^{2+}]_i$ rise induced by OAG. (A) typical traces for OAG (100 μM)-evoked $[Ca^{2+}]_i$ rises in BMSCs after treatment with siCon and siTRPC6. Traces in the upper panels are averages of more than 50 cells collected on the same day. (B) Summary of OAG-evoked $[Ca^{2+}]_i$ rise in BMSCs with siRNA treatment; average of five independent experiments (each represents 50–70 cells). **Statistically significant ($P < 0.01$) with Student's unpaired *t*-test.

Figure S4 Inhibitory effects of Gd^{3+} (1 μM) on SOC-mediated $[Ca^{2+}]_i$ rises. (A) A typical time course of SOC-mediated $[Ca^{2+}]_i$ rise and its inhibition by Gd^{3+} applied after SOCE activation; average of 63 cells. (B) Typical time course of SOC-mediated $[Ca^{2+}]_i$ rise and its inhibition by Gd^{3+} applied before SOCE activation; average of at least 50 cells evaluated on the same day. (C) Peak $[Ca^{2+}]_i$ rise of SOCE and its inhibition by Gd^{3+} applied before SOCE activation; average of at least five independent experiments (each represents the mean of 50–70 cells). **Statistically significant ($P < 0.01$) with Student's unpaired *t*-test.

Figure S5 The effect of Pyr2 (5 μM) on BMSC proliferation. For both the absence and presence of Pyr2, each data point shows the mean of five independent experiments after normalization with respect to the day 0 value. *$P < 0.05$ and **$P < 0.01$ with respect to the control (no drug; open circle), with Student's unpaired *t*-test. Control curve is the same as that shown in Figure 8.

Figure S6 The effect of TRPC6 siRNA treatment on the activation of Akt and the expression of cyclin D1 protein. siCon and siTRPC6: the same abbreviations as in Supporting Information Fig. S1. Experiments were performed 4 days after transfection of siRNA. Knockdown of TRPC6 suppressed the phosphorylation of Akt (p-Akt) without affecting the total expression of Akt protein. In contrast, the expression level of cyclin D1 protein was not affected by TRPC6 siRNA treatment. This is compatible with the unchanged cyclin D1 mRNA expression (Figure 7).

Table S1 List of conventional PCR primers specific for TRPC, STIM, Orai and cyclin isoforms. Primer pairs for TRPC1, TRPC6, STIM1, STIM2, Orai1, Orai2, Orai3, cyclinD1, cyclinE1, cyclinA2, cyclinB1 and 18SrRNA were also used for quantitative real-time PCR.